

FEYNMAN SCALING VIOLATION DUE TO BARYON NUMBER DIFFUSION IN RAPIDITY SPACE

G.H. Arakelyan*, C. Merino**, C. Pajares**, and Yu.M. Shabelski***

* A.I.Alikhanyan National Science Laboratory (Yerevan Physics Institute)
Yervan, Armenia
E-mail: argev@mail.yerphi.am

** Departamento de Física de Partículas and
Instituto Galego de Física de Altas Enerxías (IGFAE)
Universidade de Santiago de Compostela
Santiago de Compostela, Galiza, Spain
E-mail: merino@fpaxp1.usc.es
E-mail: pajares@fpaxp1.usc.es

*** Petersburg Nuclear Physics Institute
St.Petersburg, Russia
E-mail: shabelsk@thd.pnpi.spb.ru

A b s t r a c t

A significant asymmetry in baryon/antibaryon yields in the central region of high energy collisions is observed when the initial state has non-zero baryon charge. This asymmetry is connected with the possibility of a baryon charge diffusion in rapidity space. Evidently, such a diffusion should decrease the baryon charge in the fragmentation region leading to the corresponding decrease of the multiplicity of leading baryons. As a result, a new mechanism for Feynman scaling violation in the fragmentation region is obtained. We present the quantitative predictions for the Feynman scaling violation at LHC energies and even at higher energies that can be important for cosmic ray physics.

PACS. 25.75.Dw Particle and resonance production

1 Introduction

The problem of Feynman scaling violation has evident both theoretical and practical interest. In particular, this question is very important [1, 2] for cosmic ray physics, where the difference from the primary radiation to the events registered on the ground or mountain level is determined by the multiple interactions of the so-called leading particles (mainly baryons) in the atmosphere.

Despite the lack of direct measurements of Feynman scaling violation for secondary baryon spectra in nucleon-nucleon collisions at energies higher than those of ISR, some experimental information from cosmic ray experiments seems to confirm [3, 4, 5] the presence of significant Feynman scaling violation effects. Now the LHCf Collaboration has started the search [6, 7] of Feynman scaling violation effects for the spectra of photons (π^0) and neutrons in the fragmentation region at LHC energies.

In principle, the violation of Feynman scaling in the fragmentation region should exist due to the energy conservation, since the spectra of charged particles increase in the central region. However, no quantitative predictions can be made without some model of the particle production. Actually, even a small decrease of the spectrum of some secondaries in a narrow region near $x_F = 1$ may be enough to satisfy the energy conservation law.

The predictions of the Additive Quark Model [8] for Feynman scaling violation in the fragmentation region were considered in [9]. In this model, the scaling violation effects are connected with the increase of the interaction cross sections, which leads to the decrease in the number of quark-spectators which form the spectra of fast secondaries. However, to make a description of the energy dependences of the spectra as a function of x_F additional assumptions and parameters are needed.

The Quark-Gluon String Model (QGSM) [10] has some important advantages in this respect, since it is an analytical model and it allows the calculation of the spectra of secondaries at different initial energies in the whole x_F region. The QGSM is based on Dual Topological Unitarization (DTU), Regge phenomenology, and nonperturbative notions of QCD. This model is successfully used for the description of multiparticle production processes in hadron-hadron [11, 12, 13, 14], hadron-nucleus [15, 16], and nucleus-nucleus [17] collisions.

In the QGSM high energy interactions are considered as proceeding via the exchange of one or several Pomerons, and all elastic and inelastic processes result from cutting through or between Pomerons [18]. Inclusive spectra of hadrons are related to the corresponding fragmentation functions of quarks and diquarks, which are constructed using the Reggeon counting rules [19]. The quantitative predictions of the

QGSM depend on several parameters which were fixed by comparison of the theoretical calculations to the experimental data obtained at fixed target energies. The first experimental data obtained at LHC show [20] that the model predictions are in reasonable agreement with the data.

In the frame of QGSM several reasons of Feynman scaling violation in the fragmentation region exist. The first one is the increase of the average number of exchanged Pomerons with the energy, which leads to the corresponding increase of the yields of hadron secondaries in the central region and to their decrease in the fragmentation region. This effect was considered in [21, 22].

In the case of nuclear (air) targets, the growth of the hN cross section with energy leads to the increase of the average number of fast hadron inelastic collisions inside the nucleus. Thus, the average number of Pomerons is additionally increased, resulting in a stronger Feynman scaling violation [21, 22].

In reference [23] these predictions were taken into account to calculate the penetration of fast hadrons into the atmosphere, leading to a better description of the cosmic ray experimental data.

The differences in the yields of baryons and antibaryons produced in the central (midrapidity) region of high energy pp interactions [14, 20, 24, 25, 26, 27, 28] are significant. Evidently, the appearance of the positive baryon charge in the central region of pp collisions should be compensated by the decrease of the baryon multiplicities in the fragmentation region that leads to an additional reason for Feynman scaling violation.

In the present paper we consider the effects of Feynman scaling violation in pp collisions through large distance baryon diffusion in rapidity space. The role of the nuclear factor for air nuclei should be of the same magnitude as for that presented in [21, 22].

2 Baryon/antibaryon asymmetry in the QGSM

The Quark-Gluon String Model (QGSM) [10, 11, 12] allows us to make quantitative predictions of different features of multiparticle production. In QGSM the inclusive spectrum of a secondary hadron h is determined by the convolution of the diquark, valence quark, and sea quark distributions $u(x, n)$ in the incident particles with the fragmentation functions $G^h(z)$ of quarks and diquarks into the secondary hadron h . These distributions, as well as the fragmentation functions, are constructed using the Reggeon counting rules [19]. The details of the model are presented in [10, 11, 12, 14]. The Pomeron parameters were taken from [12].

In the string models, baryons are considered as configurations consisting of three connected strings (related to three valence quarks) called string junction (SJ) [29, 30, 31, 32]. Such a baryon structure is supported by lattice calculations [33]. This picture leads to some general phenomenological predictions. In the case of inclusive reactions the baryon number transfer to large rapidity distances in hadron-nucleon and hadron-nucleus reactions can be explained [14, 24, 34, 35, 36] by SJ diffusion.

The production of a baryon-antibaryon pair in the central region usually occurs via $SJ\text{-}\overline{SJ}$ (SJ has upper color indices whereas \overline{SJ} has lower indices) pair production, which then combines with sea quarks and sea antiquarks into a $B\overline{B}$ pair [31, 37], as it is shown in Fig. 1a.

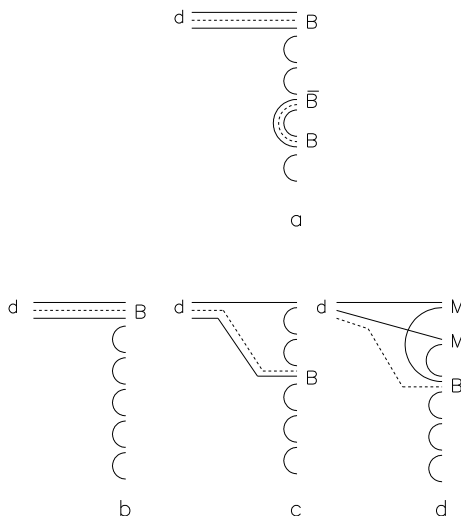


Figure 1: QGSM diagrams describing secondary baryon B production by diquark d . (a) Central production of $B\overline{B}$ pair. Single B production in the processes of diquark fragmentation: (b) initial SJ together with two valence quarks and one sea quark, (c) initial SJ together with one valence quark and two sea quarks, and (d) initial SJ together with three sea quarks. Quarks are shown by solid curves and SJ by dashed curves.

In the processes with incident baryons, e.g. in pp collisions, another possibility to produce a secondary baryon in the central region exists. This possibility is the diffusion in rapidity space of any SJ existing in the initial state and it can lead to significant differences in the yields of baryons and antibaryons in the midrapidity region even at rather high energies [14]. The most important experimental fact in favour of this process is the rather large asymmetry in Ω and $\overline{\Omega}$ baryon production in high energy π^-p interactions [38].

The theoretical quantitative description of the baryon number transfer via SJ mech-

anism was suggested in the 90's and used to predict [39] the p/\bar{p} asymmetry at HERA energies.

In order to obtain the net baryon charge we consider, following ref. [14] three different possibilities. The first one is the fragmentation of the diquark giving rise to a leading baryon (Fig. 1b). A second possibility is to produce a leading meson in the first break-up of the string and a baryon in a subsequent break-up (Fig. 1c). In these two first cases the baryon number transfer is possible only for short distances in rapidity. In the third case, shown in Fig. 1d, both initial valence quarks recombine with sea antiquarks into mesons M while a secondary baryon is formed by the SJ together with three sea quarks.

The fragmentation functions for the secondary baryon B production corresponding to the three processes shown in Figs. 1b, 1c, and 1d, can be written as follows [14]:

$$G_{qq}^B(z) = a_N \cdot v_{qq}^B \cdot z^{2.5} , \quad (1)$$

$$G_{qs}^B(z) = a_N \cdot v_{qs}^B \cdot z^2 \cdot (1 - z) , \quad (2)$$

$$G_{ss}^B(z) = a_N \cdot \varepsilon \cdot v_{ss}^B \cdot z^{1-\alpha_{SJ}} \cdot (1 - z)^2 , \quad (3)$$

where a_N is the normalization parameter, and v_{qq}^B , v_{qs}^B , v_{ss}^B are the relative probabilities for different baryons production that can be found by simple quark combinatorics [40, 41]. Their numerical values for different secondary baryons were presented in [27].

The first two processes shown in Figs. 1b and 1c, Eqs. (1) and (2), determine the spectra of leading baryons in the fragmentation region. The third contribution shown in Fig. 1d, Eq. (3), is essential if the value of the intercept of the SJ exchange Regge-trajectory, α_{SJ} , is not too small. In QGSM the weight of this third contribution is determined by the coefficient ε which fixes the small probability for such a baryon number transfer to occur.

At high energies, the SJ contribution to the inclusive cross section of secondary baryon production at large rapidity distance Δy from the incident nucleon can be estimated as

$$(1/\sigma)d\sigma^B/dy \sim a_B \cdot \varepsilon \cdot e^{(1-\alpha_{SJ})\cdot\Delta y} , \quad (4)$$

where $a_B = a_N \cdot v_{ss}^B$. The baryon charge transferred to large rapidity distances can be determined by integration of Eq. (4), so it is of the order of

$$\langle n_B \rangle \sim a_B \cdot \frac{\varepsilon}{(1 - \alpha_{SJ})} , \quad (5)$$

and so, only the left part of the initial baryon charge can be used for the production of the leading baryons.

To obtain the QGSM predictions for the spectra of leading baryons we use the standard expressions of Reggeon theory and QGSM [10, 14].

Though currently the value of $\alpha_{SJ} = 0.5$ seems more plausible [42], the value of $\alpha_{SJ} = 0.9$ can not be excluded [43, 44]. Thus, in this paper we present the calculation obtained with these two values of α_{SJ} , and also without any SJ contribution ($\varepsilon = 0.$).

3 Spectra of baryons in ep collisions

The only very high energy reaction where the leading secondary baryons were measured is ep collisions at HERA. Here, both $ep \rightarrow epX$ (i.e. $\gamma p \rightarrow pX$) [45, 46] and $ep \rightarrow enX$ (i.e. $\gamma p \rightarrow nX$) [47] were investigated at $W \sim 200$ GeV. Due to the vector dominance principle, the inelastic γp interaction can be considered as a superposition of $\rho^0 p$ and ωp^1 interactions. In the frame of the QGSM these two interactions are equivalent to the sum of $(1/2)\pi^+ p + (1/2)\pi^- p$ collisions.

In Fig. 2 the experimental data for $\gamma p \rightarrow pX$ [45, 46] and for $\gamma p \rightarrow nX$ [47] are compared with the QGSM calculations. Here the experimental data are presented as depending on x_L which is very close to x_F if p_T is small. The comparison of the $ep \rightarrow epX$ data with the QGSM calculations is shown in the upper panel of Fig. 2, while the data of the $ep \rightarrow enX$ reaction at low Q^2 and high Q^2 are presented in the middle and lower panels of Fig. 2, respectively.

The solid curves correspond to the calculations with $\alpha_{SJ} = 0.9$, dashed curves to those with $\alpha_{SJ} = 0.5$, and dotted curves are calculated without SJ contributions ($\varepsilon = 0.$). Since the energy dependences of all curves are weak, they all are calculated at $W = 200$ GeV. The difference between the curves is small. All experimental points are obtained at rather small values of the transverse momenta of the secondary baryons, so they lie below the theoretical curves that are calculated for the spectra integrated over p_T .

Usually, the spectra of neutrons produced in DIS at large x_L ($x_L \geq 0.7$) and small p_T are described in the framework of the one-pion-exchange approach [48, 49]. This approach leads to a more detailed description of the data, for example it allows one to calculate the x_L -spectra in different p_T regions. However, our QGSM description based on quark and diquark fragmentation picture gives reasonable results for $x_L \leq 0.8$.

¹As we do not consider the yields of strange secondaries, the numerically small contribution of $s\bar{s}$ pairs (ϕ -meson) is not important here.

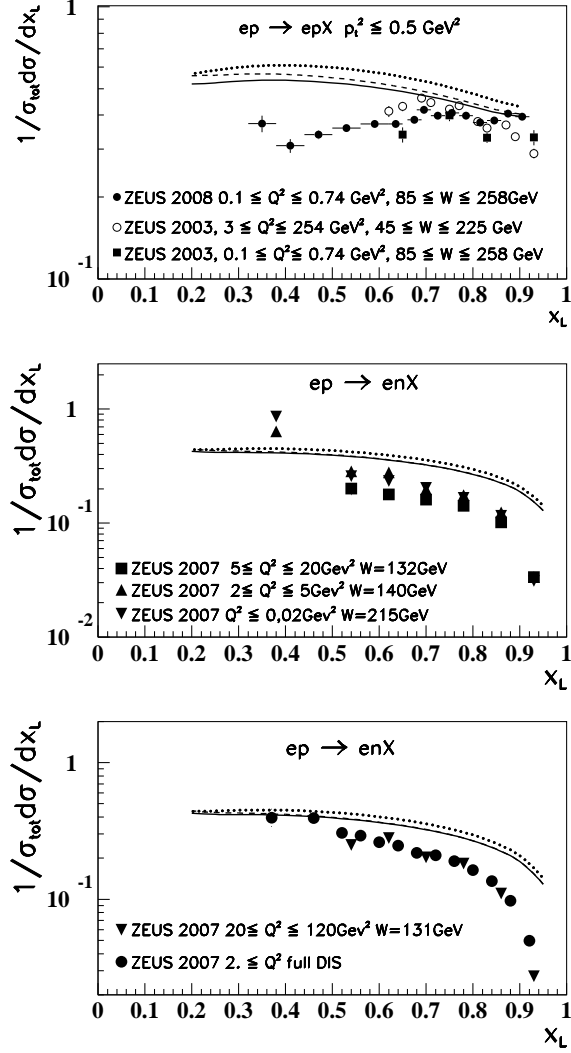


Figure 2: The QGSM predictions for the spectra of secondary protons (upper panel) and neutrons (middle and lower panels) produced in γp collisions, together with the experimental data of references [45, 46] and [47]. Solid curves correspond to the value $\alpha_{S,J} = 0.9$, dashed curves to the value $\alpha_{S,J} = 0.5$, and dotted curves are calculated without SJ contribution ($\varepsilon = 0$).

4 Predictions for the spectra of baryons in pp collisions

The QGSM predictions for the inclusive spectra of secondary protons, neutrons, and Λ at energies $\sqrt{s} = 200$ GeV, 900 GeV, 7 TeV, and 100 TeV are presented in Figs. 3, 4, and 5. In all the calculations we have accounted for the exact conservation of the baryon charge.

In all Figures 3, 4, and 5 one can see the peaks at very small x_F , that are connected

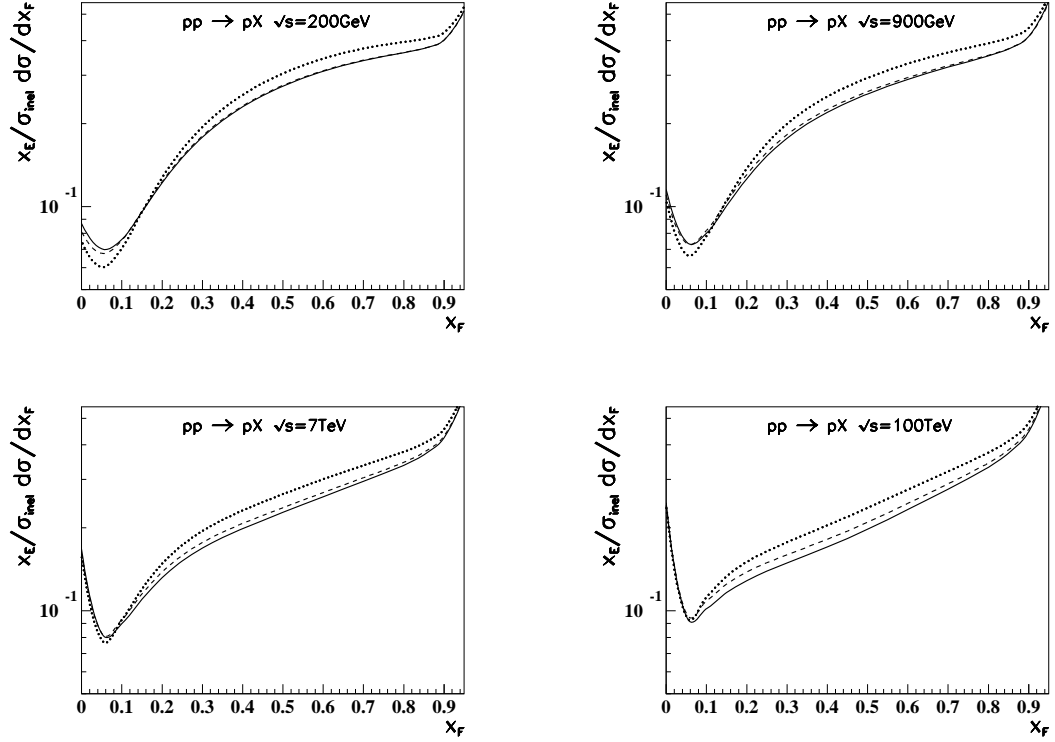


Figure 3: The QGSM predictions for the spectra of secondary protons at energies $\sqrt{s} = 200$ GeV (up left panel), $\sqrt{s} = 900$ GeV (up right panel), $\sqrt{s} = 7$ TeV (down left panel), and $\sqrt{s} = 100$ TeV (down right panel). Solid curves correspond to the value $\alpha_{SJ} = 0.9$, dashed curves to the value $\alpha_{SJ} = 0.5$, and dotted curves are calculated without SJ contribution ($\varepsilon = 0$).

to the contribution of the pair $B\bar{B}$ production via the mechanism shown in Fig. 1a. The increase of the spectra with x_F is connected to the contributions of the processes shown in Figs. 1b and 1c. The difference between both the solid and dashed curves to the dotted curves show the effect of baryon number transfer to small x_F region due to the diagram Fig. 1d. An important result is that the Feynman scaling violation is more sensitive to the fact of the inclusion of the baryon number diffusion than to the exact value of α_{SJ} .

One can see that in the case of secondary protons, shown in Fig. 3, the differences in the fragmentation region between the two calculations with SJ contribution, with values $\alpha_{SJ} = 0.9$ and $\alpha_{SJ} = 0.5$, are very small at energies $\sqrt{s} \leq 1$ TeV, while they increase up to 5-7% at higher energies. In the case of the calculations with and without SJ contribution the difference in the spectra in the region $x_F = 0.5 - 0.8$ is of about 7-10% for $\sqrt{s} = 200$ GeV and 900 GeV, and it becomes of about 15-20% at $\sqrt{s} = 7$ TeV and 100 TeV. So, by accounting for the possibility of baryon charge diffusion in rapidity space one gets one additional contribution to the Feynman scaling violation.

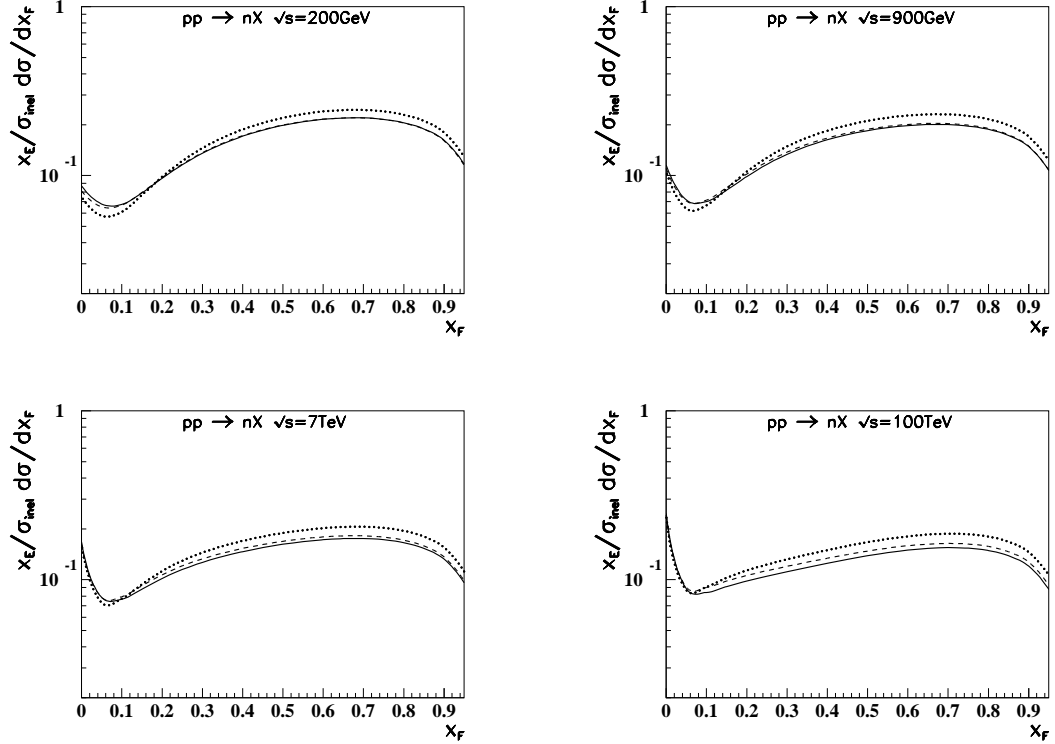


Figure 4: The QGSM predictions for the spectra of secondary neutrons at energies $\sqrt{s} = 200$ GeV (up left panel), $\sqrt{s} = 900$ GeV (up right panel), $\sqrt{s} = 7$ TeV (down left panel), and $\sqrt{s} = 100$ TeV (down right panel). Solid curves correspond to the value $\alpha_{S,J} = 0.9$, dashed curves to the value $\alpha_{S,J} = 0.5$, and dotted curves are calculated without SJ contribution ($\varepsilon = 0$).

Our predictions for the spectra of secondary neutrons are presented in Fig. 4. Their behaviour with respect to the accounting of the SJ contribution and to the effect of the Feynman scaling violation are similar to those of secondary protons.

In the case of secondary Λ -hyperon production, shown in Fig. 5, the spectra decrease rather fast at large x_F due to the faster decrease of uu and ud fragmentation functions into Λ in comparison with their fragmentation into secondary nucleon, and also to the relatively smaller contribution of diffraction dissociation. The absolute values of Λ spectra are smaller than those of the protons and neutrons spectra due to the strangeness suppression factor.

The Feynman scaling violation effects are shown in more detail in Figs. 6 and 7, for secondary protons and neutrons, respectively. Here, we present the energy dependences of the spectra at four values of x_F , namely at $x_F = 0.05$, 0.2, 0.5, and 0.7. Separately, we present for the first two values of x_F (i.e. in the top panels of Figs. 6 and 7) the energy dependences of net baryon production, i.e. the differences $p - \bar{p}$ and $n - \bar{n}$. In the case of $x_F = 0.5$ and 0.7 the differences between the baryon spectra and the

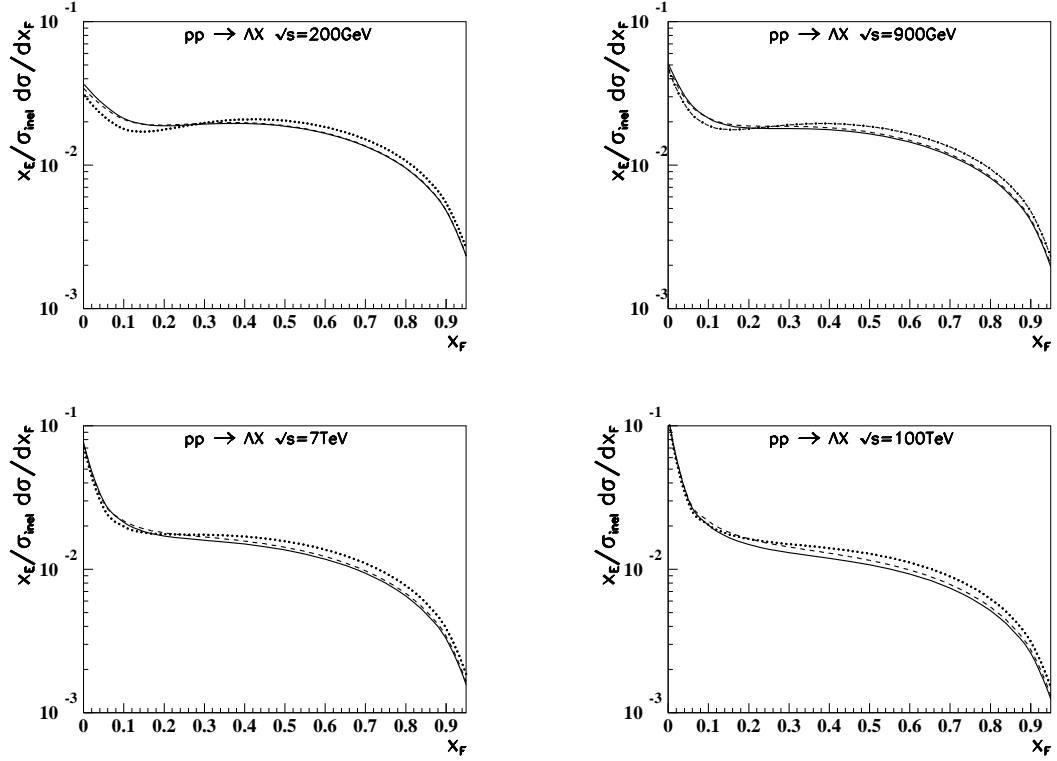


Figure 5: The QGSM predictions for the spectra of secondary Λ -hyperons at energies $\sqrt{s} = 200$ GeV (up left panel), $\sqrt{s} = 900$ GeV (up right panel), $\sqrt{s} = 7$ TeV (down left panel), and $\sqrt{s} = 100$ TeV (down right panel). Solid curves correspond to the value $\alpha_{S,J} = 0.9$, dashed curves to the value $\alpha_{S,J} = 0.5$, and dotted curves are calculated without SJ contribution ($\varepsilon = 0$).

net-baryon spectra are negligible.

One can see that at $x_F = 0.05$ and 0.2 the spectra of secondary protons and neutrons increase with energy (both the total spectra as well as the net baryon spectra). At larger x_F these spectra decrease with the energy. These energy dependences are connected with the growth of the average number of exchanging Pomerons. The differences between solid and dashed curves to dotted curves show the effect of SJ diffusion.

5 The ratios of the inclusive spectra of baryons at different energies

The possible Feynman scaling violation at superhigh energies was discussed in [6], based on Monte Carlo calculations. These effects are, as a rule, numerically not large, and so it is more suitable to consider the ratios of the spectra at different energies.

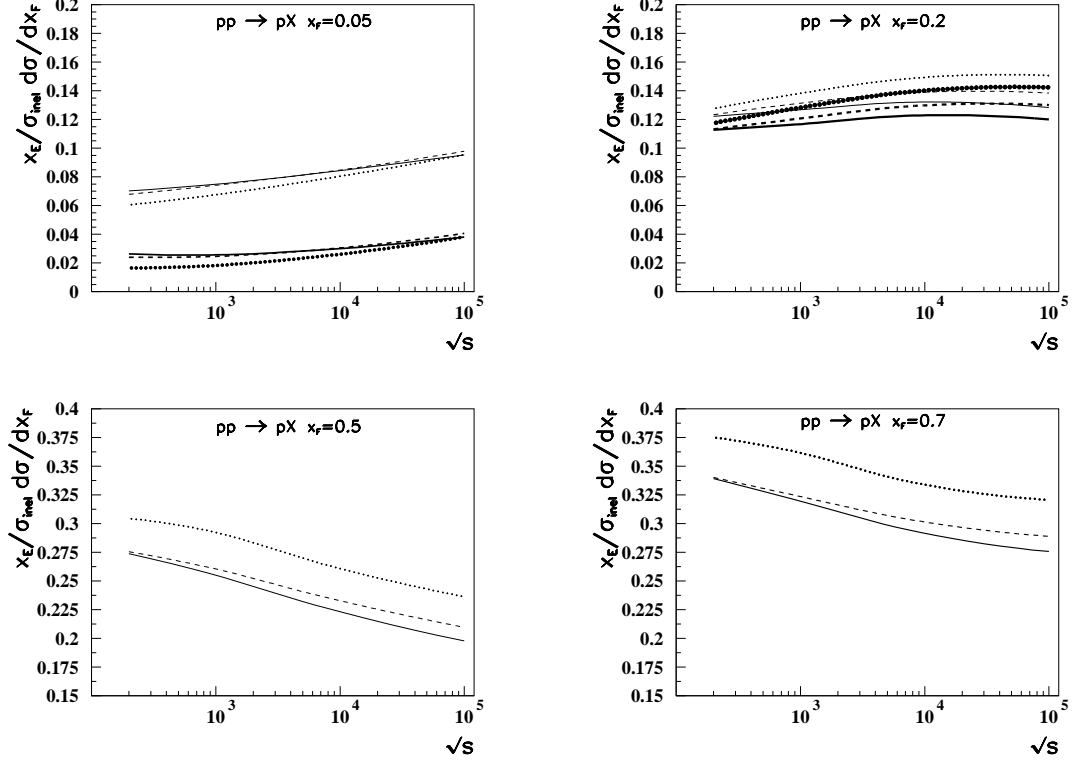


Figure 6: The QGSM predictions for the spectra of secondary protons as the functions of energy at fixed values of x_F . Thin curves show the total proton spectra and bold curves at top panels the spectra of net protons, i.e. the values of the $p - \bar{p}$ differences. Solid curves correspond to the value $\alpha_{SJ} = 0.9$, dashed curves to the value $\alpha_{SJ} = 0.5$, and dotted curves are calculated without SJ contribution ($\varepsilon = 0$).

These ratios calculated in the QGSM at $\sqrt{s} = 7$ TeV, 14 TeV, and 1000 TeV to the values at $\sqrt{s} = 900$ GeV, are presented both for secondary protons and neutrons in Fig. 8.

In Fig. 9 we present the ratios of the spectra of secondary protons and neutrons as the functions of rapidity, calculated with $\alpha_{SJ} = 0.9$ and without SJ contribution, at $\sqrt{s} = 200$ GeV (solid curves) and at $\sqrt{s} = 100$ TeV (dashed curves). The similar ratios calculated with $\alpha_{SJ} = 0.5$ and without SJ contribution are shown by dash-dotted curves at $\sqrt{s} = 200$ GeV and by dotted curves at $\sqrt{s} = 100$ TeV.

6 Conclusion

We present the QGSM predictions for Feynman scaling violation in the spectra of leading baryons due to baryon charge diffusion at large distances in the rapidity space.

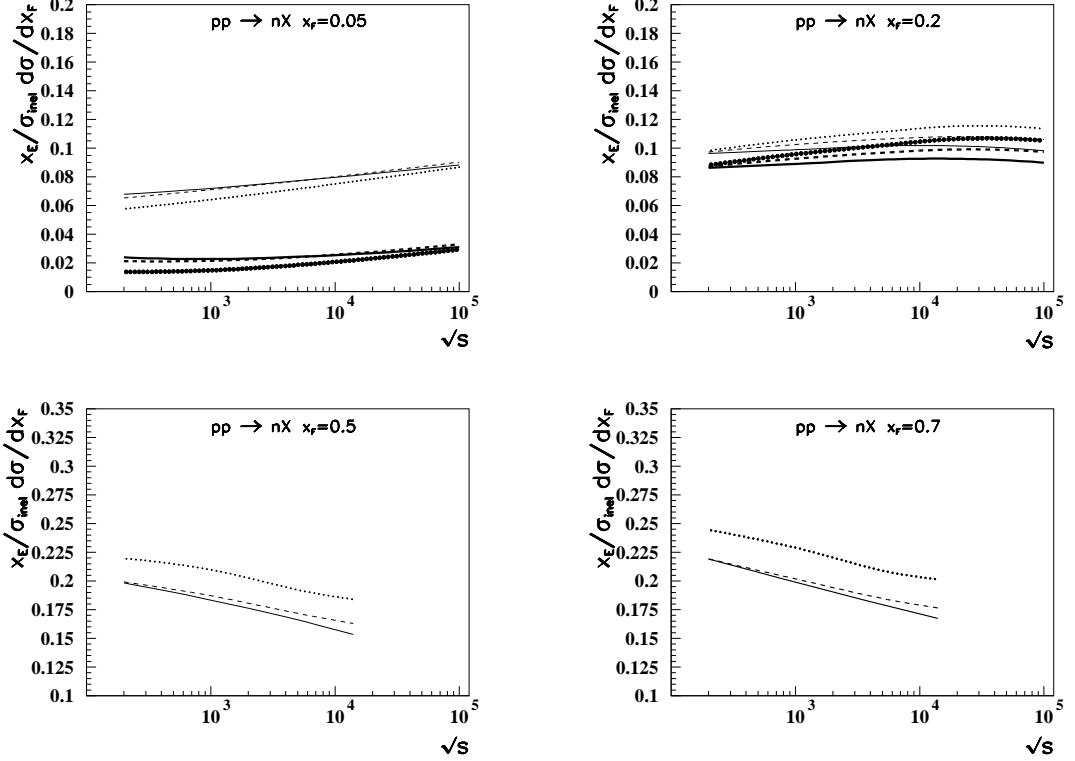


Figure 7: The QGSM predictions for the spectra of secondary neutrons as the functions of energy at fixed values of x_F . Thin curves show the total neutron spectra and bold curves at top panels the spectra of net neutrons, i.e. the values of $n - \bar{n}$ differences. Solid curves correspond to the value $\alpha_{SJ} = 0.9$, dashed curves to the value $\alpha_{SJ} = 0.5$, and dotted curves are calculated without SJ contribution ($\varepsilon = 0$).

The existence of such a diffusion has been attested observed in many papers, even at the LHC energies, and so the decrease of the spectra in the fragmentation region is the direct consequence of baryon charge conservation. However, the numerical values of the scaling violation at different x_F are model-dependent. On the other point of view, the calculations of scaling violation for leading baryons should be accompanied by the calculation of the baryon/antibaryon asymmetry in the central region.

The first experimental data obtained at LHC are in general agreement with the QGSM calculations performed with the same values of parameters which were determined at lower energies (mainly for the description of the the fixed target experiments). However, the numerical value of α_{SJ} is not well-known. ALICE Collaboration data on the ratios of $\bar{p}p$ production are in agreement with a value $\alpha_{SJ} = 0.5$, while LHCb Collaboration data on the ratios of $\bar{\Lambda}\Lambda$ production do not allow to fix the value of α_{SJ} , and there are two experimental results for $\bar{B}B$ production asymmetry.

We neglect by the possibility of interactions between Pomerons the (so-called en-

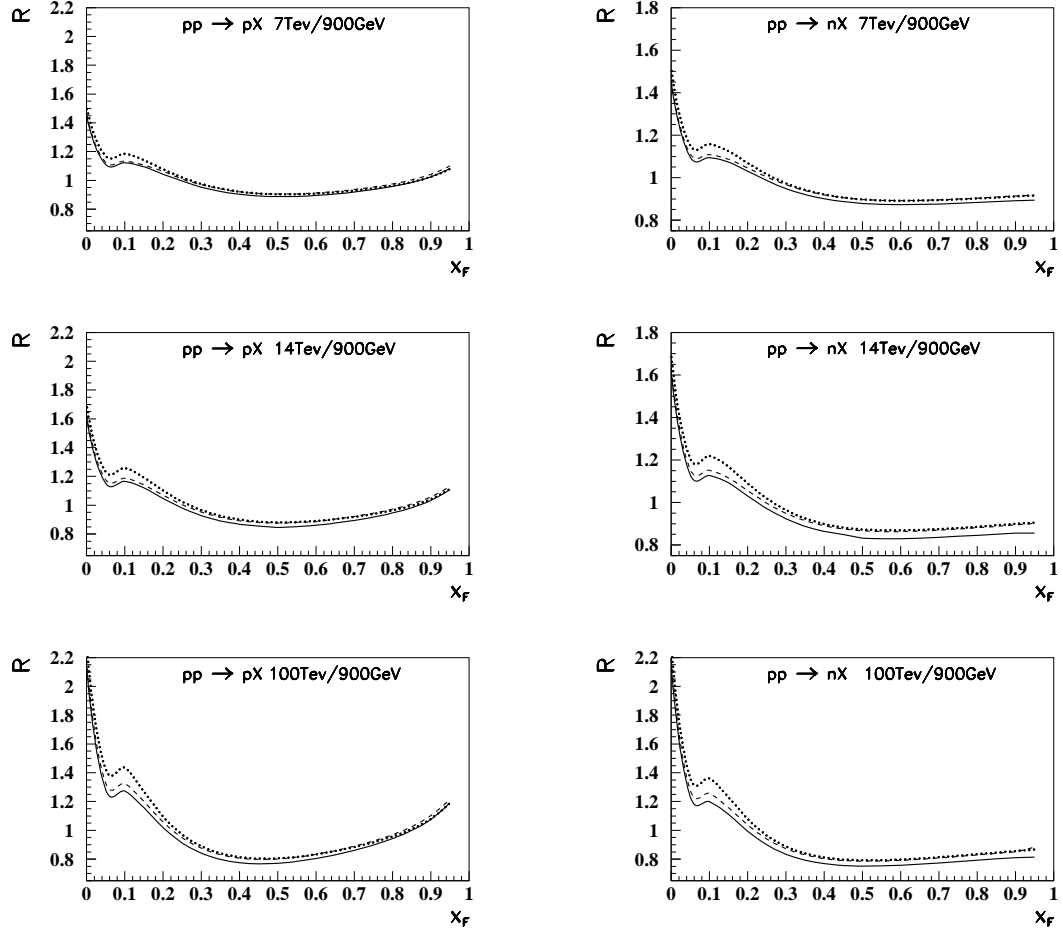


Figure 8: The QGSM predictions for the ratios of the spectra of secondary protons (left panels) and neutrons (right panels) at three different energies to those at $\sqrt{s} = 900$ GeV.

hancement diagrams), since our estimations [50] show that the inclusive density of secondaries produced in pp collisions at LHC energies is not large enough for these diagrams to be significant.

Our calculations are in reasonable agreement with the results of ref. [51].

Acknowledgements

We are grateful to [A.B. Kaidalov](#) for useful discussions and comments. This paper was supported by Ministerio de Educación y Ciencia of Spain under the Spanish Consolider-Ingenio 2010 Programme CPAN (CSD2007-00042) and project FPA 2005–01963, by Xunta de Galicia, Spain, and, in part, by grant RFBR 11-02-00120-a and by the Department of Education and Science of the Republic of Armenia, Grant-11-1C015.

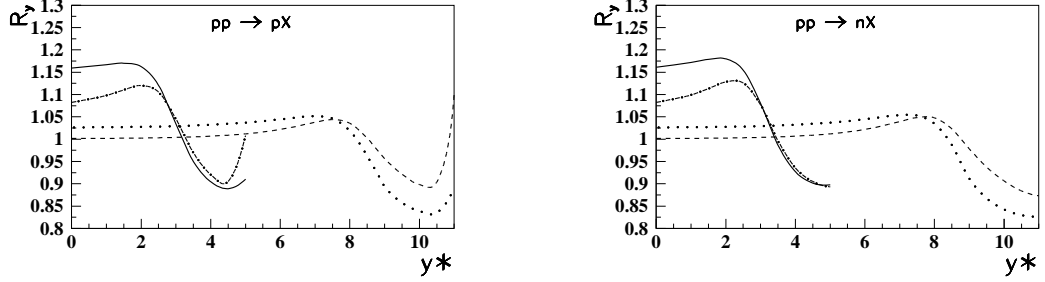


Figure 9: The QGSM predictions for the ratios of the spectra of secondary protons (left panels) and neutrons (right panels) calculated with $\alpha_{S,J} = 0.9$ (solid and dashed curves) and with $\alpha_{S,J} = 0.9$ (dash-dotted and dotted curves) and with energies $\sqrt{s} = 200$ GeV (solid and dash-dotted curves) and at $\sqrt{s} = 100$ TeV (dashed and dotted curves).

References

- [1] J. Abraham et al., Phys. Rev. Lett. **104**, 091101 (2010) and arXiv:1002.0699 [astro-ph.HE].
- [2] R.U. Abbasi et al., Phys. Rev. Lett. **104**, 161101 (2010) and arXiv:0910.4184 [astro-ph.HE].
- [3] E.L. Feinberg, Phys. Rep. **50**, 237 (1972).
- [4] S.N. Vernov et al., J. Phys **C3**, 1601 (1977).
- [5] M.N. Kalmykov and G.B. Khistiansen, JETP Lett. **37**, 247 (1983).
- [6] T. Sako, LHCf Collaboration, arXiv:1010.0195 [hep-ex].
- [7] O. Adriani et al., LHCf Collaboration, arXiv:1012.1490 [hep-ex].
- [8] V.V. Anisovich, Yu.M. Shabelski, and V.M. Shekhter, Nucl. Phys. B **5133**, 477 (1978).
- [9] V.V. Anisovich, V.M. Braun, and Yu.M. Shabelski, Z. Phys. C **27**, 77 (1985).
- [10] A.B. Kaidalov and K.A. Ter-Martirosyan, Yad. Fiz. **39**, 1545 (1984); **40**, 211 (1984).
- [11] A.B. Kaidalov and O.I. Piskounova, Yad. Fiz. **41**, 1278 (1985); Z. Phys. **C30**, 145 (1986).

- [12] Yu.M. Shabelski, *Yad. Fiz.* **44**, 186 (1986).
- [13] F. Anselmino, L. Cifarelli, E. Eskut, and Yu.M. Shabelski, *Nouvo Cim.* **105A**, 1371 (1992).
- [14] G.H. Arakelyan, A. Capella, A.B. Kaidalov, and Yu.M. Shabelski, *Eur. Phys. J. C* **26**, 81 (2002) and hep-ph/0103337.
- [15] A.B. Kaidalov, K.A. Ter-Martirosyan, and Yu.M. Shabelski, *Yad. Fiz.* **43**, 1282 (1986).
- [16] Yu.M. Shabelski, *Z. Phys.* **C38**, 569 (1988).
- [17] J. Dias de Deus and Yu.M. Shabelski, *Yad. Fiz.* **71**, 191 (2008).
- [18] V.A. Abramovsky, V.N. Gribov, and O.V. Kancheli, *Yad. Fiz.* **18**, 595 (1973).
- [19] A.B. Kaidalov, *Sov. J. Nucl. Phys.* **45**, 902 (1987); *Yad. Fiz.* **43**, 1282 (1986).
- [20] C. Merino, C. Pajares, M.M. Ryzhinskiy, and Yu.M. Shabelski, arXiv:1007.3206[hep-ph].
- [21] Yu.M. Shabelski, *Yad. Fiz.* **45**, 223 (1987).
- [22] Yu.M. Shabelski, *Z. Phys.* **C38**, 569 (1988).
- [23] A.D. Erlykin, N.P. Krutikova, and Yu.M. Shabelski, *Yad. Fiz.* **45** 1075 (1987), **47** 1667 (1988).
- [24] F. Bopp and Yu.M. Shabelski, *Yad. Fiz.* **68**, 2155 (2005) and hep-ph/0406158; *Eur. Phys. J. A* **28**, 237 (2006) and hep-ph/0603193.
- [25] G.H. Arakelyan, C. Merino, C. Pajares, and Yu.M. Shabelski, *Eur. Phys. J.* **C54**, 577 (2008) and hep-ph/0709.3174.
- [26] C. Merino, M.M. Ryzhinskiy, and Yu.M. Shabelski, *Eur. Phys. J.* **C62**, 491 (2009); arXiv:0810.1275 [hep-ph].
- [27] G.H. Arakelyan, A.B. Kaidalov, C. Merino, and Yu.M. Shabelski, *Phys. Atom. Nucl.* **74**, 426 (2011) and arXiv:1004.4074 [hep-ph].
- [28] C. Merino, C. Pajares, and Yu.M. Shabelski, *Eur. Phys. J.* **C71**, 1652 (2011); arXiv:1105.3174 [hep-ph].
- [29] X. Artru, *Nucl. Phys. B* **85**, 442 (1975).

- [30] M. Imachi, S. Otsuki, and F. Toyoda, Prog. Theor. Phys. **52**, 346 (1974); **54**, 280 (1976); **55**, 551 (1976).
- [31] G.C. Rossi and G. Veneziano, Nucl. Phys. B **123**, 507 (1977).
- [32] D. Kharzeev, Phys. Lett. B **378**, 238 (1996).
- [33] V.G. Bornyanov et al., Uspekhi Fiz. Nauk. **174**, 19 (2004).
- [34] G.H. Arakelyan, C. Merino, and Yu.M. Shabelski, Yad. Fiz. **69**, 911 (2006) and hep-ph/0505100; Phys. Atom. Nucl. **70**, 1110 (2007) and hep-ph/0604103; Eur. Phys. J. **A31**, 519 (2007) and hep-ph/0610264.
- [35] O.I. Piskounova, Phys. Atom. Nucl. **70**, 1110 (2007) and hep-ph/0604157.
- [36] C. Merino, M.M. Ryzhinskiy, and Yu.M. Shabelski, Proceedings of the XLIII PNPI Winter School on Nuclear and Particle Physics (PNPI-2009), Repino, St.Petersburg, Russia, February 24th-March 1st, 2009, pages 156-185, and arXiv:0906.2659 [hep-ph].
- [37] S.E. Vance, M. Gyulassy, and X-N. Wang, Phys. Lett. B **443**, 45 (1998).
- [38] E.M. Aitala *et al.*, E769 Collaboration, hep-ex/0009016; Phys. Lett. B **469**, 9 (2000).
- [39] B.Z. Kopeliovich and B. Povh, Z. Phys. C **75**, 693 (1997); Phys. Lett. B **446**, 321 (1999).
- [40] V.V. Anisovich and V.M. Shekhter, Nucl. Phys. B **55**, 455 (1973).
- [41] A. Capella and C.A. Salgado, Phys. Rev. C **60**, 054906 (1999).
- [42] K. Aamodt et al., ALICE Collaboration, Phys. Rev. Lett. **105**, 072002 (2010) and arXiv:1006.5432 [hep-ex].
- [43] F. Dettori, LHCb Collaboration, hep-ex/1009.1221.
- [44] C. Merino, C. Pajares, and Yu.M. Shabelski, Proceedings of the International Conference on Hadron Structure and QCD, Gatchina (2010), to appear.
- [45] S. Chekanov et al., ZEUS Collaboration, Nucl. Phys. **B658**, 3 (2003) and hep-ex/0210029.
- [46] S. Chekanov et al., ZEUS Collaboration, JHEP **0906**, 74 (2009) and arXiv:0812.2416 [hep-ex].

- [47] S. Chekanov et al., ZEUS Collaboration, Nucl. Phys. **B776**, 1 (2007) and hep-ex/0702028.
- [48] A B. Kaidalov et al., Eur. Phys. J. **C47**, 385 (2006).
- [49] B.Z. Kopeliovich et al., Phys. Rev. **D78**, 014031 (2008) and arXiv:0805.4534 [hep-ph].
- [50] C. Merino, C. Pajares, and Yu.M. Shabelski, Eur. Phys. J. **C59**, 691 (2009) and arXiv:0802.2195 [hep-ph].
- [51] C.J. Bleibel et al., arXiv:1011.2703 [hep-ex].